



Contents lists available at SciVerse ScienceDirect

Chemical Engineering Science

journal homepage: www.elsevier.com/locate/ces

Dynamics and control of aggregate thin film surface morphology for improved light trapping: Implementation on a large-lattice kinetic Monte Carlo model

Jianqiao Huang^a, Xinyu Zhang^a, Gerassimos Orkoulas^a, Panagiotis D. Christofides^{a,b,*}

^a Department of Chemical and Biomolecular Engineering, University of California, Los Angeles, CA 90095, USA

^b Department of Electrical Engineering, University of California, Los Angeles, CA 90095, USA

ARTICLE INFO

Article history:

Received 16 July 2011

Received in revised form

5 August 2011

Accepted 9 August 2011

Available online 18 August 2011

Keywords:

Surface morphology

Light trapping optimization

Model predictive control

Distributed parameter systems

Thin film growth

Thin film solar cells

ABSTRACT

This work demonstrates the use of feedback control, coupled with a suitable actuator design, in manufacturing thin films whose surface morphology is characterized by a desired visible light reflectance/transmittance level. The problem is particularly important in the context of thin film manufacturing for thin film solar cells where it is desirable to produce thin films with precisely tailored light trapping characteristics. Initially, a thin film deposition process involving atom adsorption and surface migration is considered and is modeled using a large-lattice (lattice size=40,000) kinetic Monte Carlo simulation. Subsequently, thin film surface morphology characteristics like roughness and slope are computed with respect to different characteristic length scales ranging from atomic to the ones corresponding to visible light wavelength and it is found that a patterned actuator design is needed to induce thin film surface roughness and slope at visible light wavelength spatial scales, which lead to desired thin film reflectance and transmittance levels. Then, an Edwards–Wilkinson-type equation (a second-order stochastic partial differential equation) is used to model the surface evolution at the visible light wavelength spatial scale and form the basis for the design of a feedback controller whose objective is to manipulate the deposition rate across the spatial domain of the process. The model parameters of the Edwards–Wilkinson equation are estimated from kinetic Monte Carlo simulations and their dependence on the deposition rate is used in the formulation of the predictive controller to predict the influence of the control action on the surface roughness and slope throughout the thin film growth process. Analytical solutions of the expected surface roughness and surface slope at the visible light wavelength spatial scale are obtained by solving the Edwards–Wilkinson equation and are used in the control action calculation. The cost function of the controller involves penalties on both surface roughness and slope from set-point values as well as constraints on the magnitude and rate of change of the control action. The controller is applied to the large-lattice kinetic Monte Carlo simulation. Simulation results demonstrate that the proposed controller and patterned actuator design successfully regulate aggregate surface roughness and slope to set-point values at the end of the deposition that yield desired levels of thin film reflectance and transmittance.

© 2011 Elsevier Ltd. All rights reserved.

1. Introduction

Thin film solar cells constitute an important and growing component of the overall solar cell market (see, for example, Green, 2007; van Sark et al., 2007) owing to their reduced cost relative to silicon-based solar cell modules as well as to the potential of using various thin film materials which may lead to improved light conversion efficiencies (currently on the order of 10% for production modules). In addition to investigating the performance with respect to light conversion efficiency and long-term

stability of an array of materials, thin film solar cell technology stands to benefit from optimal thin film manufacturing (deposition) control strategies that produce thin films with desired light reflectance and transmittance properties. Specifically, extensive research on optical properties of thin film, primarily silicon, solar cells has demonstrated that the scattering properties of the thin film interfaces directly influence the light trapping ability and the efficiency of thin film silicon solar cells (see, for example, Zeman and Vanswaaij, 2000; Poruba et al., 2000; Muller and Rech, 2004; Rowlands et al., 2004). Shaping the morphology of the various surfaces and interfaces at the thin film deposition stage is therefore critical in order to maximize the amount of light trapped within the solar cell and converted to electrical energy. With respect to visible light trapping by thin film solar cells, the light scattering properties of the various surfaces/interfaces have a complex dependence on

* Corresponding author at: Department of Chemical and Biomolecular Engineering, University of California, Los Angeles, CA 90095, USA.

Tel.: +1 310 794 1015; fax: +1 310 206 4107.

E-mail address: pdc@seas.ucla.edu (P.D. Christofides).

the surface morphology interface. While developing accurate models for predicting optical properties of thin films is an on-going research topic, it is well-established that the root-mean-square surface roughness and slope at characteristic length scales that are comparable to the wavelength of the visible light are key factors that influence thin film reflectance and transmittance (e.g., Davies, 1954; Vorburger et al., 1993). Specifically, significant increase of conversion efficiency with appropriately roughened interfaces has been reported in several works (Tao and Zeman, 1994; Leblanc and Perrin, 1994; Springer and Poruba, 2001; Krč and Zeman, 2002; Isabella et al., 2010). Despite the importance of these efforts and the broad realization that surface morphology could be tailored to improve thin film solar cell efficiency, the problem of shaping thin film surface morphology during film deposition by appropriately controlling the surface slope and roughness to desired levels has received limited attention. Thus, it is desirable to develop systematic approaches to manufacture thin film solar cells with optimal light conversion efficiencies via computational multiscale modeling and real-time model-based control of the manufacturing process.

Over the last 20 years within the control engineering literature, extensive efforts have been made on the modeling and model-based feedback control of thin film deposition processes with emphasis on the problems of film thickness, roughness and porosity regulation. Microscopic modeling of thin film growth is usually carried out via kinetic Monte Carlo (kMC) methods (see, for example, Gillespie, 1976; Reese et al., 2001; Christofides et al., 2008 for results and references in this area) as well as stochastic partial differential equations (e.g., Edwards and Wilkinson, 1982; Vvedensky et al., 1993; Lauritsen et al., 1996). With respect to model-based feedback control of thin film deposition, early efforts focused on deposition spatial uniformity control on the basis of continuum-type distributed parameter models (e.g., Christofides, 2001), while within the last 10 years, most attention has focused on control of thin film surface morphology and microstructure. Since kMC models are not available in closed form and cannot be readily used for feedback control design and system-level analysis, stochastic differential equation (SDE) models (whose parameters are computed from kMC model data) have been used as the basis for the design of feedback controllers to regulate thin film surface roughness (e.g., Christofides et al., 2008; Ni and Christofides, 2005; Varshney and Armaou, 2005, 2006; Hu et al., 2009a), film porosity (Hu et al., 2009a, 2009b), and film thickness (Hu et al., 2009c). In an attempt to manufacture thin film solar cells with optimal light conversion efficiencies, we recently initiated an effort toward modeling and control of thin film surface morphology to optimize thin film light reflectance and transmittance properties. To this end, we initially studied the dynamics and lattice size dependence of surface mean slope (Huang et al., 2010b) and developed predictive control algorithms to regulate both surface roughness and slope at an atomic level using stochastic PDEs in one spatial dimension (Zhang et al., 2010b) and two spatial dimensions (Zhang et al., 2010a). Taking advantage of these analysis and controller design results, we recently (Zhang et al., in press) made the first attempt to control thin film surface morphology at a length scale comparable to the visible light wavelength. Specifically, we addressed aspects of this problem with respect to predictive controller design using a stochastic PDE with a patterned deposition rate profile but we did not address the challenging problem of implementing the predictive controller on a large-lattice kinetic Monte Carlo simulation that can cover a significant number of visible light wavelengths (which is on the order of 400 nm–700 nm).

Motivated by the above considerations, this work presents an integrated control actuator and control algorithm design for the regulation of deposition of thin films such that the final thin film surface morphology is characterized by a desired visible light

reflectance/transmittance level. To demonstrate the approach, we focus on a thin film deposition process involving atom adsorption and surface migration and use a large-lattice (lattice size=40,000) kinetic Monte Carlo simulation to describe its spatiotemporal behavior; this allows computing surface roughness and slope at different length scales ranging from atomic scale to visible light wavelength scale. Subsequently, thin film surface morphology characteristics like roughness and slope are computed for different characteristic length scales and it is found that a patterned actuator design is needed to induce thin film surface roughness and slope at visible light wavelength spatial scales, that lead to desired thin film reflectance and transmittance values. Since a large-lattice kinetic Monte Carlo model cannot be used as the basis for controller design and real-time controller calculations, an Edwards–Wilkinson-type equation is used to model the surface evolution at the visible light wavelength spatial scale and to form the basis for feedback controller design within a model predictive control framework. The cost function of the predicted controller involves penalties on both surface roughness and slope from set-point values as well as constraints on the magnitude and rate of change of the control action. The Edwards–Wilkinson equation model parameters are estimated from kinetic Monte Carlo simulations and their dependence on the manipulated input (deposition rate) is used to predict the influence of the control action on the surface roughness and slope during the growth process. The controller formulation takes advantage of analytical solutions of the expected surface roughness and surface slope at the visible light wavelength spatial scale and the controller is applied to the large-lattice kinetic Monte Carlo simulation. Extensive simulation studies demonstrate that the proposed controller and patterned actuator design successfully regulate surface roughness and slope at visible light wavelength spatial scales to set-point values at the end of the deposition that yield desired levels of thin film reflectance and transmittance.

2. Thin film deposition process description and modeling

In this section, a one-dimensional solid-on-solid (SOS) on-lattice kinetic Monte Carlo (kMC) model is used to simulate the thin film deposition process, which includes two microscopic processes: an adsorption process, in which particles are incorporated onto the film from the gas phase, and a migration process, in which surface particles move to adjacent sites (Levine et al., 1998; Levine and Clancy, 2000; Wang and Clancy, 2001; Yang et al., 1997). The model is valid for temperatures $T < 0.5T_m$, where T_m is the melting point of the deposited material (Levine et al., 1998). At high temperatures ($T \lesssim T_m$), the particles cannot be assumed to be constrained on the lattice sites and the on-lattice model may not be valid. In this work, a square lattice is selected to represent the structure of the film, as shown in Fig. 1. All particles are modeled as identical hard spheres and the centers of the particles deposited on the film are located on the lattice sites. The diameter of the particles equals the distance between two neighboring sites. The width of the lattice is fixed so that the lattice contains a fixed number of sites in the lateral direction. The new particles are always deposited from the top side of the lattice with vertical incidence; see Fig. 1. Particle deposition results in film growth in the direction normal to the lateral direction. The direction normal to the lateral direction is thus designated as the growth direction. The number of sites in the lateral direction is defined as the lattice size and is denoted by L . Periodic boundary conditions (PBCs) are applied at the edges of the lattice in the lateral direction.

The top particles of each column are defined as the surface particles and the positions of the centers of all surface particles form the surface height profile. The number of nearest neighbors

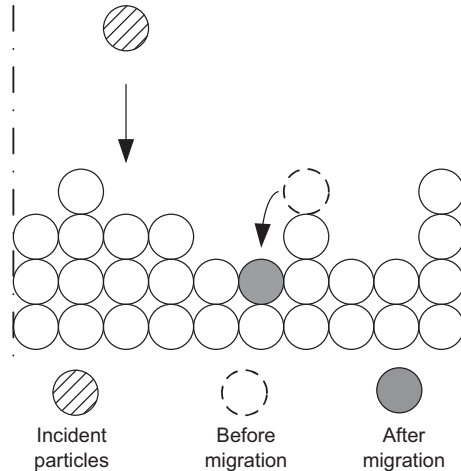


Fig. 1. Thin film growth process on a solid-on-solid one-dimensional square lattice.

of a surface particle ranges from zero to two. A surface particle with zero nearest neighbors is possible to migrate to one of its adjacent columns with equal probability. A surface particle with one nearest neighbor is possible to migrate to its adjacent column with lower height with appropriate probability based on the migration rate (please see Eq. (1)). A surface particle with two nearest neighbors cannot migrate. Particles that are not on the film surface can not migrate.

In the adsorption process, a site is randomly selected with uniform probability among all lattice sites and a particle is deposited on top of this site. The overall adsorption rate, w , is expressed in the unit of layer per second. In the migration process, a surface particle overcomes the energy barrier of the site and jumps to a vacant neighboring site. The migration rate (probability) of a particle follows an Arrhenius-type law with a pre-calculated activation energy barrier that depends on the local environment of the particle, i.e., the number of the nearest neighbors of the particle chosen for a migration event. The migration rate of the i th surface particle is calculated as follows:

$$r_m = v_0 \exp\left(-\frac{E_s + n_i E_n}{k_B T}\right), \quad (1)$$

where v_0 denotes the pre-exponential factor, n_i is the number of the nearest neighbors of the i th particle and can take the values of 0 and 1, (r_m is zero when $n_i=2$ since in the one-dimensional lattice this surface particle is fully surrounded by other particles and cannot migrate), E_s is the contribution to the activation energy barrier from the site itself, E_n is the contribution to the activation energy barrier from each nearest neighbor, k_B is Boltzmann's constant and T is the substrate temperature of the thin film. Since the film is thin, the temperature is assumed to be uniform throughout the film.

2.1. Surface morphology at atomic level

Thin film surface morphology, which can be expressed in terms of surface roughness and slope, is a very important surface property influencing the light trapping properties of thin films. Surface roughness is defined as the root-mean-square (RMS) of the surface height profile. Specifically, the definition of surface roughness is given as follows:

$$r = \left[\frac{1}{L} \sum_{i=1}^L (h_i - \bar{h})^2 \right]^{1/2}, \quad (2)$$

where r denotes the surface roughness, h_i , $i=1, 2, \dots, L$, is the surface height at the i th position in the unit of layer, L denotes the lattice size, and the surface mean height is given by $\bar{h} = (1/L) \sum_{i=1}^L h_i$.

In addition to the surface roughness, another quantity that also determines the surface morphology is the surface mean slope. In this work, the surface mean slope is defined as the RMS of the surface gradient profile as follows:

$$m = \left[\frac{1}{L} \sum_{i=1}^L h_{s,i}^2 \right]^{1/2}, \quad (3)$$

where m denotes the RMS slope and $h_{s,i}$ is the surface slope at the i th lattice site, which is a dimensionless variable. The surface slope, $h_{s,i}$ is computed as follows:

$$h_{s,i} = \frac{h_{i+1} - h_i}{1}. \quad (4)$$

Since the unit of height is layer and the distance between two adjacent particles (the diameter of particles) always equal to one layer, the denominator of $h_{s,i}$ is always one. Due to the use of PBCs, the slope at the boundary lattice site ($i=L$) is computed as the slope between the last lattice site (h_L) and the first lattice site (h_1).

To investigate the open-loop properties of surface morphology, a set of kMC simulations is carried out at different w with $T=480$ K and $L=40,000$. In particular, the continuous-time Monte Carlo (CTMC) method is used in the kMC simulations. In this method, a list of events is constructed and an event is selected randomly with its respective probability. After the execution of the selected event, the list is updated based on the new lattice configuration. The following values are used for the parameters of the migration rate of Eq. (1), $v_0 = 10^{13} \text{ s}^{-1}$, $E_s = 1.2 \text{ eV}$ and $E_n = 0 \text{ eV}$. Figs. 2 and 3 show that both atomic roughness and slope increase with time and approach steady-state values at different time scales. Furthermore, both surface roughness and slope increase with deposition rate w . It is important to note that surface roughness and slope are correlated to some extent in the deposition process, but they are separate variables that describe different aspects of the film surface. Films with the same surface roughness may have different mean slope values.

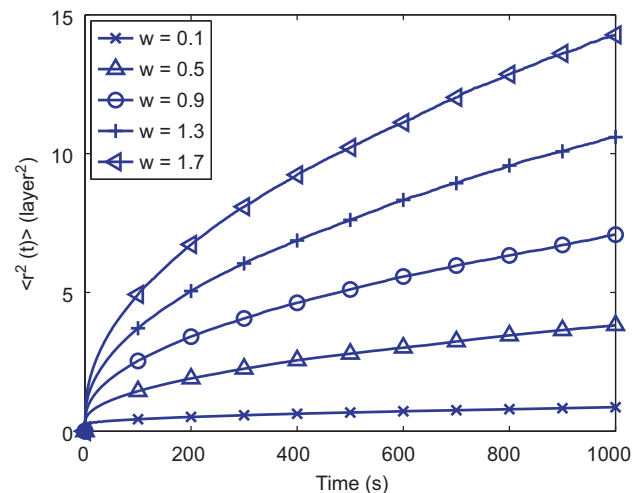


Fig. 2. Evolution of expected atomic surface roughness with respect to time for different deposition rates (unit of w is layer/s) obtained from kMC simulations.

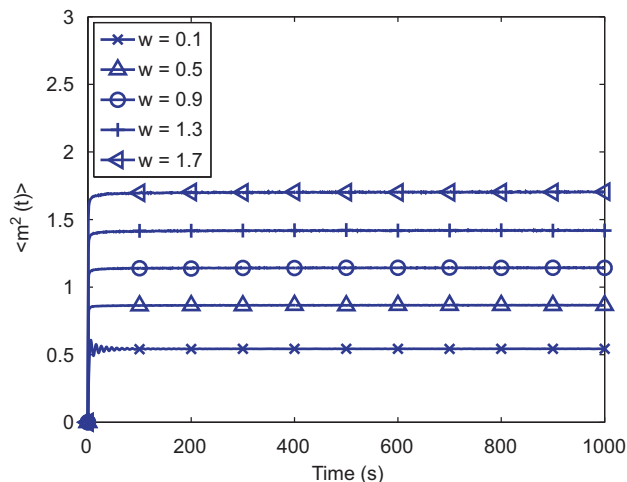


Fig. 3. Evolution of expected atomic surface slope with respect to time for different deposition rates (unit of w is layer/s) obtained from kMC simulations.

2.2. Aggregate surface morphology and spatial deposition rate profile

One of the most important applications of our work is to simulate and control the deposition process of thin film solar cells in order to improve solar cell efficiency via enhanced light trapping. However, the wavelength of visible light (400 nm–700 nm) is much larger than the diameter of silicon atoms (~ 0.25 nm) and thus, it is necessary to define an aggregate surface morphology at length scales comparable to visible light wavelength.

Specifically, the aggregate surface morphology is computed similar to the atomic surface morphology, but on the basis of the aggregate surface height profile, $h_{A,i}$, which is defined as follows:

$$h_{A,i} = (h_{i\Delta+1} + h_{i\Delta+2} + \dots + h_{(i+1)\Delta}) / \Delta, \quad i = 0, 1, \dots, L/\Delta - 1, \quad (5)$$

where $h_{A,i}$ denotes the averaged surface height over the length scale of Δ sites, Δ denotes the aggregation size, i.e., the number of lattice sites used to calculate the aggregate surface height, and L/Δ denotes the number of aggregate sites of size Δ included in the spatial domain of the process. For the wavelength of visible light and silicon thin film solar cells, the corresponding Δ is around 400; this follows from the fact that $0.25 \text{ nm} \cdot 400 = 100 \text{ nm}$, which is a length scale comparable to visible light wavelength. The definition of aggregate surface roughness and slope is given as follows:

$$r_A = \left[\frac{1}{L} \sum_{i=1}^{L/\Delta} (h_{A,i} - \bar{h}_A)^2 \right]^{1/2},$$

$$m_A = \left[\frac{1}{L} \sum_{i=1}^{L/\Delta} \left(\frac{h_{A,i} - h_{A,i+1}}{\Delta} \right)^2 \right]^{1/2}. \quad (6)$$

The dynamics of the aggregate surface roughness and slope are dependent on the characteristic length scale, Δ . To investigate this dependence, kMC simulations with $E_n = 0$ eV and $L = 40,000$ were carried out. The expected aggregate surface roughness square, $\langle r_A^2(t) \rangle$, and the expected aggregate surface slope square, $\langle m_A^2(t) \rangle$, are calculated from the aggregate surface height profile from kMC simulations for different aggregation lengths. The simulation duration is $t_f = 1000$ s and 100 independent simulations were carried out to calculate the expected values of aggregate surface roughness and slope. Figs. 4 and 5 show the profiles of aggregate surface roughness square and slope square for different characteristic length scales, Δ . It is clear that the larger the characteristic length scale, the smaller

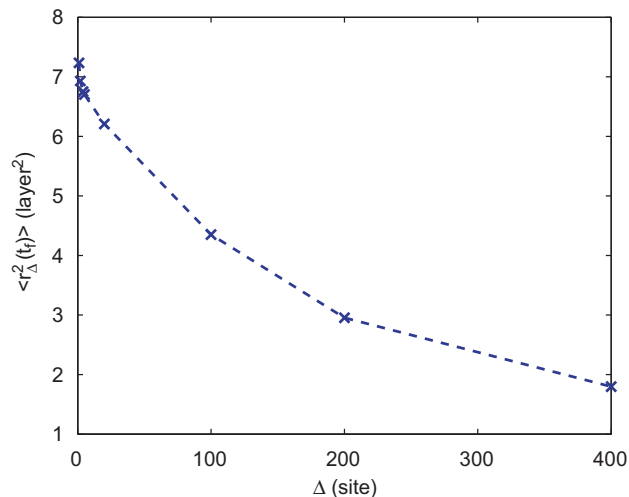


Fig. 4. Dependence of expected aggregate surface roughness on aggregation size obtained from kMC simulations; $t_f = 1000$ s.

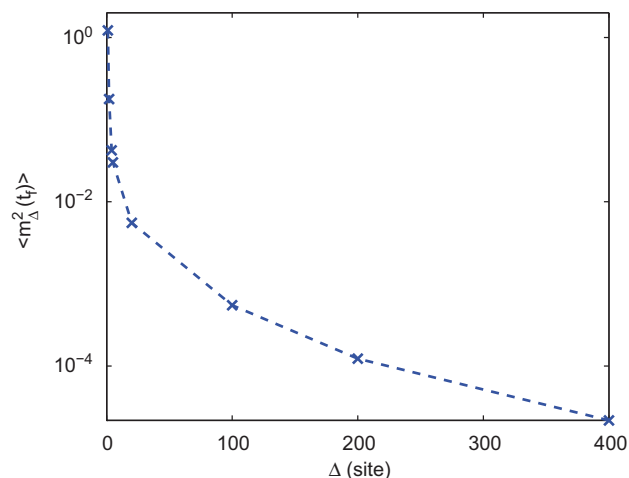


Fig. 5. Dependence of expected aggregate surface slope on aggregation size obtained from kMC simulations; $t_f = 1000$ s.

the aggregate roughness and slope square. Furthermore, Fig. 5 shows that as the aggregation size increases, the aggregate slope square decreases very fast; a much weaker dependence is observed for aggregate roughness in Fig. 4. From these results, we see that the corresponding aggregate slope square for $\Delta = 400$ is very small ($\langle m_A^2 \rangle_{ss} \sim 10^{-5}$). This close-to-zero value of aggregate slope square reveals a smoothly changing surface profile with respect to characteristic length scales that are comparable to visible light wavelength. The smoothness of the surface profile persists at larger lattice sizes as well, due to the very weak lattice-size dependence of the mean slope square. This small aggregate slope square at large characteristic length scales is partly because the operating conditions are spatially uniform throughout the entire deposition process, i.e., the same deposition rate and substrate temperature are applied throughout the spatial domain. Thus, a spatially non-uniform deposition rate profile is necessary for the purpose of optimizing thin film light reflectance/transmittance by manipulation of film aggregate surface roughness and slope at length scales comparable to visible light wavelength; this conclusion is also

consistent with recent experimental data (Isabella et al., 2010). To this end, we introduce a patterned in space deposition rate profile, which is defined as follows:

$$w(x) = w_0 + A \sin\left(\frac{2k\pi}{L}x\right), \quad 0 \leq A \leq w_0, \quad (7)$$

where x is a position along the lattice, w_0 is the mean deposition rate, A is the magnitude of the patterned deposition profile, k is the number of sine waves along the entire lattice, and L is the lattice size. Referring to the difference between w and w_0 , it is necessary to point out that w_0 is the mean deposition rate of the patterned deposition rate profile, $w(x)$, while the w used in Section 2.1 is a spatially-uniform deposition rate.

The dynamics of aggregate surface morphology with patterned deposition rate profile is studied by carrying out a series of simulations at different mean deposition rates w_0 with $L=40,000$, $\Delta=400$, $T=480$ K, $k=5$ and $A=0.1w_0$. The evolution profiles are shown in Figs. 6 and 7. The introduction of patterned deposition rate profiles significantly changes the dynamic profiles

of aggregate surface morphology. However, some properties of uniform deposition rate evolution profiles remain valid, for example, the expected values of aggregate surface roughness and slope still increase with mean deposition rate w_0 . Furthermore, simulations are carried out at $w_0=1$ layer/s with different magnitude, A , values to investigate the influence of the strength of patterned deposition on the evolution profiles of aggregate surface morphology. As shown in Figs. 8 and 9, the magnitude, A , has substantial influence on the dynamics of aggregate surface morphology. Both aggregate roughness and aggregate slope can be increased by 10,000 times by manipulating A compared to the aggregate surface morphology achieved with a uniform deposition rate profile. Thus, the introduction of a patterned deposition rate profile substantially expands the range of surface morphology values that can be obtained and makes light trapping optimization at length scales comparable to visible light wavelength possible. Finally, referring to the influence of the migration activation energy values on the aggregate surface roughness and slope steady state values, we note that such an influence exists

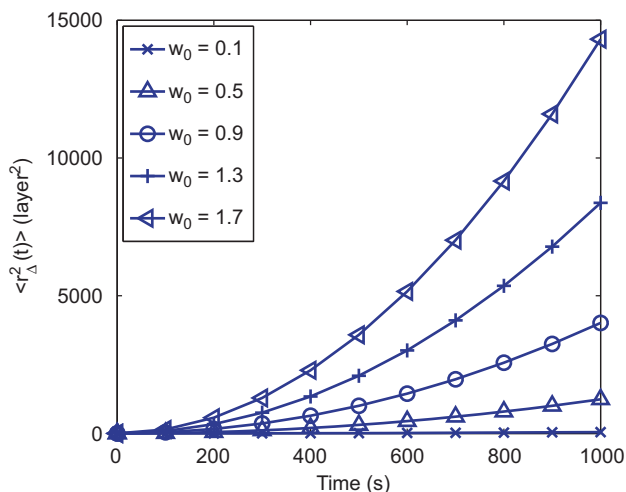


Fig. 6. Evolution of expected aggregate surface roughness with respect to time for different mean deposition rates (unit of w_0 is layer/s) obtained from kMC simulations. Patterned deposition with $k=5$ and $A=0.1w_0$.

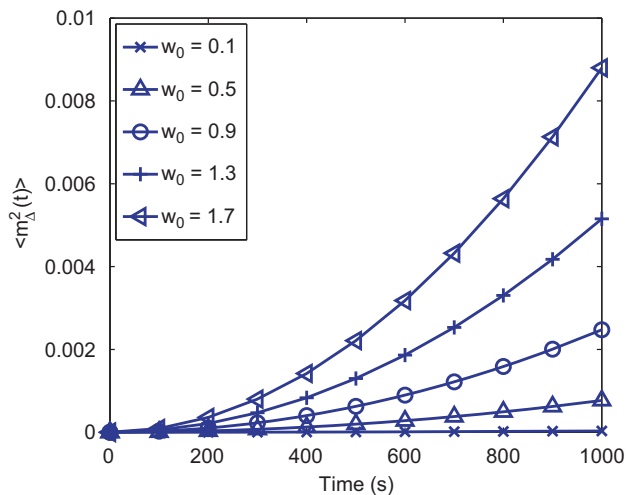


Fig. 7. Evolution of expected aggregate surface slope with respect to time for different mean deposition rates (unit of w_0 is layer/s) obtained from kMC simulations. Patterned deposition with $k=5$ and $A=0.1w_0$.

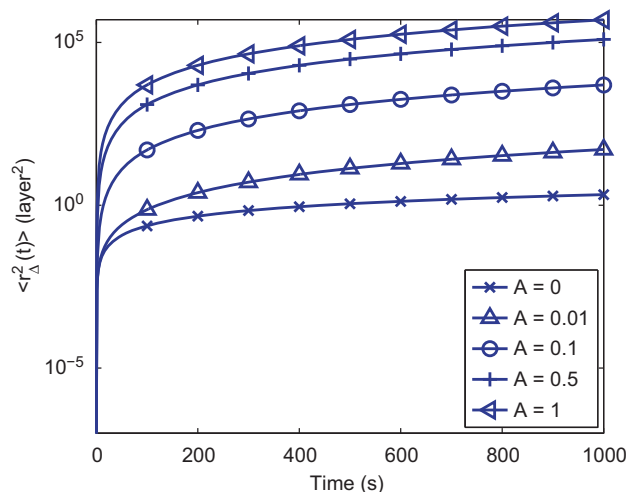


Fig. 8. Evolution of expected aggregate surface roughness with respect to time for different patterned deposition rate magnitudes obtained from kMC simulations. Patterned deposition with $k=5$ and $w_0=1$ layer/s.

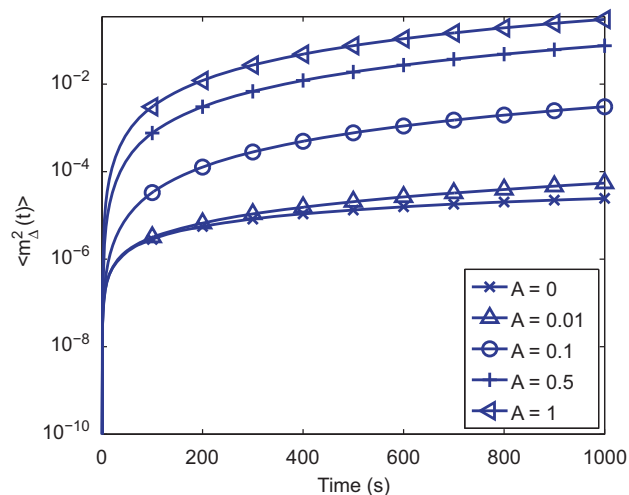


Fig. 9. Evolution of expected aggregate surface slope with respect to time for different patterned deposition rate magnitudes obtained from kMC simulations. Patterned deposition with $k=5$ and $w_0=1$ layer/s.

but it is small at aggregation levels corresponding to visible light wavelength.

3. Closed-form modeling and parameter estimation

3.1. Edward–Wilkinson-type equation of aggregate surface height

Given the complexity of the deposition process and the need to control surface roughness and slope at spatial scales comparable to the wavelength of visible light, the direct computation of a closed-form model, describing the surface height evolution and is suitable for controller design, from the microscopic deposition mechanisms is a very difficult (if not impossible) task. Therefore, a hybrid modeling approach should be used in which a basic closed-form modeling structure is used and the model parameters are computed such that the predictions of key variables from the closed-form model are close to the one of the kinetic Monte Carlo model for a broad set of operating conditions. To this end, we use an Edward–Wilkinson (EW)-type equation, which is a second-order stochastic PDE to describe the aggregate surface height evolution and compute its parameters from kMC data. The choice of the EW-equation is motivated by the fact that it has been used in many deposition processes that involve a thermal balance between adsorption (deposition) and migration (diffusion) (Buzea and Robbie, 2005). Specifically, a one-dimensional EW-type equation is used to describe the evolution of aggregate surface height profile:

$$\frac{\partial h_A}{\partial t} = w(x,t) + c_2 \frac{\partial^2 h_A}{\partial x^2} + \zeta(x,t) \quad (8)$$

subject to the following periodic boundary conditions

$$h_A(0,t) = h_A(L,t), \quad (9)$$

$$\frac{\partial h_A}{\partial x}(0,t) = \frac{\partial h_A}{\partial x}(L,t) \quad (10)$$

and the initial condition

$$h_A(x,0) = h_A^0(x), \quad (11)$$

where $x \in [0,L]$ is the spatial coordinate, t is the time, $h_A(x,t)$ is the aggregate surface height and $\zeta(x,t)$ is a Gaussian white noise with zero mean and the following covariance:

$$\langle \zeta(x,t)\zeta(x',t') \rangle = \sigma^2 \delta(x-x')\delta(t-t'), \quad (12)$$

where $\delta(\cdot)$ denotes the Dirac delta function. In Eq. (8), the parameters c_2 and σ^2 , corresponding to diffusion effects and stochastic noise, respectively, depend on the deposition rate $w(x,t)$. In the case of a patterned deposition rate profile (control actuation), the term $w(x,t)$ is of the form:

$$w(x,t) = w_0(t) + A(t)\sin\left(\frac{2k\pi}{L}x\right), \quad (13)$$

where $w_0(t)$ is the mean deposition rate, $A(t)$ is the magnitude of patterned deposition rate, and k is the number of sine waves between 0 and L .

To analyze the dynamics and obtain a solution of the EW equation suitable for real-time controller calculations, we first consider the eigenvalue problem of the linear operator of Eq. (8) subject to the periodic boundary conditions of Eqs. (9)–(10):

$$A\bar{\phi}_n(x) = c_2 \frac{d^2 \bar{\phi}_n(x)}{dx^2} = \lambda_n \bar{\phi}_n(x), \quad (14)$$

$$\nabla^j \bar{\phi}_n(0) = \nabla^j \bar{\phi}_n(L), \quad j = 0, 1, \quad (15)$$

where λ_n denotes an eigenvalue, $\bar{\phi}_n$ denotes an eigenfunction, and $\nabla^j, j=0, 1$, denotes the gradient of a given function. The solution of

the eigenvalue problem of Eqs. (14)–(15) is as follows:

$$\lambda_n = -\frac{4c_2\pi^2 n^2}{L^2}, \quad (16)$$

$$\phi_{1,n}(x) = \phi_n = \sqrt{\frac{2}{L}} \sin\left(\frac{2n\pi}{L}x\right), \quad (17)$$

$$\phi_{2,n}(x) = \psi_n = \begin{cases} \sqrt{\frac{1}{L}} & n = 0, \\ \sqrt{\frac{2}{L}} \cos\left(\frac{2n\pi}{L}x\right) & n \neq 0. \end{cases} \quad (18)$$

The solution of the EW equation of Eq. (8) can be expanded in an infinite series in terms of the eigenfunctions of the operator of Eq. (14) as follows:

$$h_A(x,t) = \sum_{n=0}^{L/(2A)} (\phi_{1,n}(x)z_{1,n}(t) + \phi_{2,n}(x)z_{2,n}(t)), \quad (19)$$

where $z_{1,n}(t), z_{2,n}(t)$ are time-varying coefficients.

Substituting the above expansion for the solution, $h_A(x,t)$, into Eq. (8) and taking the inner product with the adjoint eigenfunctions, the following system of infinite stochastic linear ordinary differential equations (ODEs) for the temporal evolution of the time-varying coefficients in Eq. (19) is obtained:

$$\frac{dz_{2,0}(t)}{dt} = w_{2,0} + \zeta_{2,0}(t), \quad (20)$$

$$\frac{dz_{p,n}(t)}{dt} = w_{p,n} + \lambda_n z_{p,n} + \zeta_{p,n}(t), \quad p = 1, 2, \quad n = 1, \dots, \frac{L}{2A}, \quad (21)$$

where $\zeta_{p,n}(t) = \int_0^L \zeta(x,t)\phi_{p,n}(x) dx$ is the projection of the noise $\zeta(x,t)$ on the ODE for $z_{p,n}$. The noise term, $\zeta_{p,n}$, has zero mean and covariance

$$\langle \zeta_{p,n}(t)\zeta_{p,n}(t') \rangle = \sigma^2 \delta(t-t'). \quad (22)$$

Similarly, $w_{p,n}$ is the projection of w on the ODE for $z_{p,n}(t)$, $w_{p,n} = \int_0^L \phi_{p,n}(x)w(x) dx$

- If $p=1$,

$$w_{1,n} = \begin{cases} 0, & n \neq k, \\ A\sqrt{\frac{L}{2}}, & n = k. \end{cases} \quad (23)$$

- If $p=2$,

$$w_{2,n} = \begin{cases} 0, & n \neq 0, \\ A\sqrt{L}, & n = 0. \end{cases} \quad (24)$$

The temporal evolution of the variance of mode $z_{p,n}$ can be obtained from the solution of the linear ODEs of Eqs. (20) and (21) as follows:

$$\langle z_{2,0}(t) \rangle = w_{2,0}(t-t_0), \quad (25)$$

$$\text{var}(z_{2,0}(t)) = \sigma^2(t-t_0), \quad (26)$$

$$\langle z(t) \rangle = e^{\lambda(t-t_0)} \langle z(t_0) \rangle + \frac{w_p}{\lambda} (e^{\lambda(t-t_0)} - 1), \quad (27)$$

$$\text{var}(z(t)) = e^{2\lambda(t-t_0)} \text{var}(z(t_0)) + \sigma^2 \frac{e^{2\lambda(t-t_0)} - 1}{2\lambda}, \quad (28)$$

where $z(t) = z_{p,n}(t)$, $\lambda = \lambda_n$ and $w_p = w_{p,n}$ for $n \neq 0$.

Finally, it is necessary to point out that, when aggregate (discrete) surface height profile is used, the highest number of modes that can be accurately estimated from $h_A(x,t)$ is limited by

the spatial sampling points, $n \leq L/2\Delta$; the reader may refer to Zhang et al. (in press) for a detailed discussion of this issue.

3.2. Aggregate surface root-mean-square roughness

Aggregate surface roughness of the thin film is defined as the standard deviation of the aggregate surface height profile from its average height

$$r_A(t) = \sqrt{\frac{1}{L} \int_0^L [h_A(x,t) - \bar{h}_A(t)]^2 dx}, \quad (29)$$

where $\bar{h}_A(t) = (1/L) \int_0^L h_A(x,t) dx$ is the average aggregate surface height. According to Eq. (19), we have

$$\bar{h}_A(t) = \frac{1}{L} \int_0^L \phi_{2,0} z_{2,0} dx = \sqrt{\frac{1}{L}} z_{2,0}. \quad (30)$$

Using that

$$h_A(x,t) - \bar{h}_A(t) = \sum_{n=1}^{L/(2\Delta)} \sum_{p=1}^2 \phi_{p,n}(x) z_{p,n}(t) \quad (31)$$

the expected aggregate surface roughness, $\langle r_A^2(t) \rangle$, of Eq. (29) can be re-written as

$$\begin{aligned} \langle r_A^2(t) \rangle &= \left\langle \frac{1}{L} \int_0^L \left[\sum_{p=1}^2 \sum_{n=1}^{L/(2\Delta)} z_{p,n}(t) \phi_{p,n}(x) \right]^2 dx \right\rangle \\ &= \left\langle \frac{1}{L} \int_0^L \sum_{n=1}^{L/(2\Delta)} (\phi_{1,n}^2(x) z_{1,n}^2(t) + \phi_{2,n}^2(x) z_{2,n}^2(t)) dx \right\rangle \\ &= \frac{1}{L} \sum_{n=1}^{L/(2\Delta)} (\langle z_{1,n}^2 \rangle + \langle z_{2,n}^2 \rangle), \end{aligned} \quad (32)$$

where

$$\langle z_{p,n}^2 \rangle = \text{var}(z_{p,n}) + \langle z_{p,n} \rangle^2. \quad (33)$$

The expression of Eqs. (32)–(33) will be used in the MPC formulation; please see Eq. (42).

3.3. Aggregate surface root-mean-square slope

The aggregate RMS slope is defined as the root-mean-square of the aggregate surface slope in the x -direction as follows:

$$\begin{aligned} m_A(t) &= \sqrt{\frac{1}{L} \int_0^L \left(\frac{\partial h_A}{\partial x} \right)^2 dx} \\ &= \sqrt{\frac{1}{L} \sum_{i=0}^{L/\Delta} \left(\frac{h_A(i+1,t) - h_A(i,t)}{\Delta} \right)^2 \Delta}. \end{aligned} \quad (34)$$

Using the expansion of Eq. (19), Eq. (34) can be written as:

$$\begin{aligned} \langle m_A^2(t) \rangle &= \left\langle \frac{1}{L} \sum_{i=0}^{L/\Delta} \left(\frac{h_A(i+1,t) - h_A(i,t)}{\Delta} \right)^2 \Delta \right\rangle \\ &= \left\langle \frac{1}{L\Delta} \sum_{i=0}^{L/\Delta} \left\{ \sum_{p=1}^2 \sum_{n=0}^{L/(2\Delta)} z_{p,n} [\phi_{p,n}(i+1) - \phi_{p,n}(i)] \right\}^2 \right\rangle \\ &= \left\langle \frac{1}{L\Delta} \sum_{i=0}^{L/\Delta} \sum_{p_1=1}^2 \sum_{n_1=0}^{L/(2\Delta)} \sum_{p_2=1}^2 \sum_{n_2=0}^{L/(2\Delta)} z_{p_1,n_1} z_{p_2,n_2} d\phi_{p_1,n_1}(i) d\phi_{p_2,n_2}(i) \right\rangle \\ &= \frac{1}{L\Delta} \sum_{p_1=1}^2 \sum_{n_1=0}^{L/(2\Delta)} \sum_{p_2=1}^2 \sum_{n_2=0}^{L/(2\Delta)} \langle z_{p_1,n_1} z_{p_2,n_2} \rangle \left(\sum_{i=0}^{L/\Delta} d\phi_{p_1,n_1}(i) d\phi_{p_2,n_2}(i) \right), \end{aligned} \quad (35)$$

where

$$\sum_{i=0}^{L/\Delta} d\phi_{p_1,n_1}(i) d\phi_{p_2,n_2}(i)$$

$$\begin{aligned} &= \sum_{i=0}^{L/\Delta} (\phi_{p_1,n_1}(i+1) - \phi_{p_1,n_1}(i)) (\phi_{p_2,n_2}(i+1) - \phi_{p_2,n_2}(i)) \\ &= \frac{2}{L} \left(\sum_{i=0}^{L/\Delta} \left(\sin\left(\frac{2n_1\pi}{L/\Delta}(i+1)\right) - \sin\left(\frac{2n_1\pi}{L/\Delta}i\right) \right) \left(\sin\left(\frac{2n_2\pi}{L/\Delta}(i+1)\right) - \sin\left(\frac{2n_2\pi}{L/\Delta}i\right) \right) \right) \\ &= \frac{8}{L} \sin\left(\frac{n_1\pi}{L/\Delta}\right) \sin\left(\frac{n_2\pi}{L/\Delta}\right) \sum_{i=0}^{L/\Delta} \left(\cos\left(\frac{n_1\pi}{L/\Delta}(2i+1)\right) \cos\left(\frac{n_2\pi}{L/\Delta}(2i+1)\right) \right) \end{aligned} \quad (36)$$

or more compactly:

$$\begin{aligned} \langle m_A^2(t) \rangle &= \frac{1}{L\Delta} \sum_{p_1=1}^2 \sum_{n_1=0}^{L/(2\Delta)} \sum_{p_2=1}^2 \sum_{n_2=0}^{L/(2\Delta)} \langle z_{p_1,n_1} z_{p_2,n_2} \rangle \left(\sum_{i=0}^{L/\Delta} d\phi_{p_1,n_1}(i) d\phi_{p_2,n_2}(i) \right) \\ &= \frac{1}{L\Delta} \sum_{p=1}^2 \sum_{n=0}^{L/(2\Delta)} \langle z_{p,n} \rangle^2 \left(\frac{8}{L} \sin^2\left(\frac{n\pi}{L/\Delta}\right) \sum_{i=0}^{L/\Delta} \left(\cos^2\left(\frac{n\pi}{L/\Delta}(2i+1)\right) \right) \right) \\ &= \sum_{p=1}^2 \sum_{n=0}^{L/(2\Delta)} K_{p,n} \langle z_{p,n}^2 \rangle, \end{aligned} \quad (37)$$

where

$$\begin{aligned} K_{p,n} &= \frac{8}{L\Delta} \sin^2\left(\frac{\pi n}{L/\Delta}\right) \sum_{i=0}^{L/(2\Delta)} \left(\cos^2\left(\frac{n\pi}{L/\Delta}(2i+1)\right) \right) \\ &= \begin{cases} \frac{8}{L\Delta} \sin^2\left(\frac{\pi n}{L/\Delta}\right) & n=0, \\ \frac{4}{L\Delta} \sin^2\left(\frac{\pi n}{L/\Delta}\right) & n \neq 0. \end{cases} \end{aligned} \quad (38)$$

Finally, using that

$$\begin{aligned} &\sum_{i=0}^{L/(2\Delta)} \left(\cos^2\left(\frac{n\pi}{L/\Delta}(2i+1)\right) \right) \\ &= \sum_{i=0}^{L/(2\Delta)} \left(\frac{\cos(2n\pi(2i+1)/(L/\Delta)) + 1}{2} \right) \\ &= \begin{cases} \frac{L}{\Delta} & \text{if } n=0, \\ \frac{L}{2\Delta} & \text{if } n \neq 0. \end{cases} \end{aligned} \quad (39)$$

$\langle m_A^2(t) \rangle$ can be expressed as:

$$\langle m^2(t) \rangle = \sum_{m=1}^{L/(2\Delta)} (K_{1,m} \langle z_{1,m}^2 \rangle + K_{2,m} \langle z_{2,m}^2 \rangle). \quad (40)$$

The expression of Eq. (40) will be used in the MPC formulation; please see Eq. (42).

3.4. Parameter estimation

Referring to the EW equation of Eq. (8), there are two model parameters, c_2 and σ^2 that must be determined as functions of the mean deposition rate w_0 and of the patterned deposition rate magnitude A . These parameters affect the dynamics of aggregate surface roughness and slope and can be estimated by fitting the predicted evolution profiles for aggregate surface roughness and slope from the EW equation to profiles of aggregate surface roughness and slope from kMC simulations. Least-square methods are used to estimate the model parameters so that the EW-model predictions are close in a least-square sense to the kMC simulation data. Comparison of the predictions of both models is shown in Fig. 10. It is necessary to point out that 20 groups of EW-equation-simulations are carried out with mean deposition rate w_0 ranging from $w_0=0.1$ layer/s to $w_0=2$ layer/s, but in Fig. 10 only five groups of simulation results are shown. Based on c_2 and

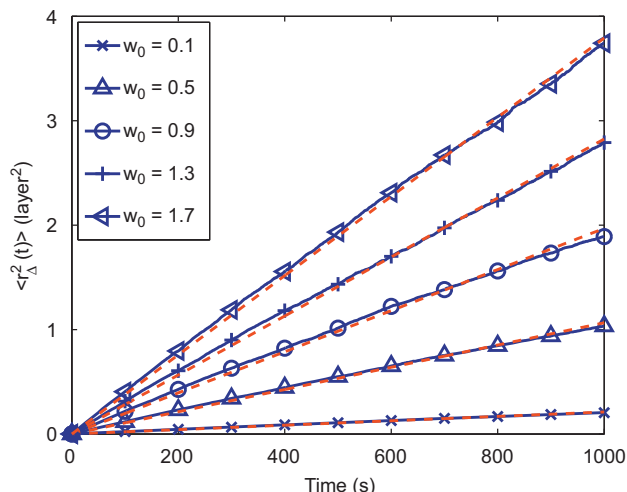


Fig. 10. Evolution of expected aggregate surface roughness with respect to time for different spatially uniform deposition rates obtained from kMC simulations (solid lines with symbols). The analytical solutions for the aggregate surface roughness obtained from the corresponding EW equations with the fitted values for c_2 and σ^2 are also shown (dashed lines).

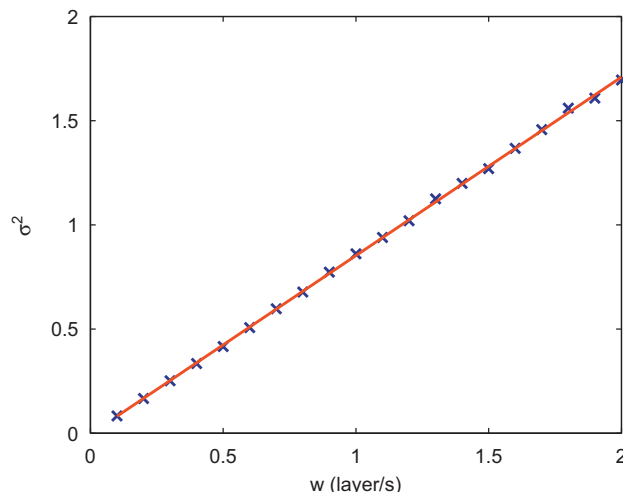


Fig. 12. σ^2 values for different spatially uniform deposition rates w . The solid line is the result of a linear fitting function.

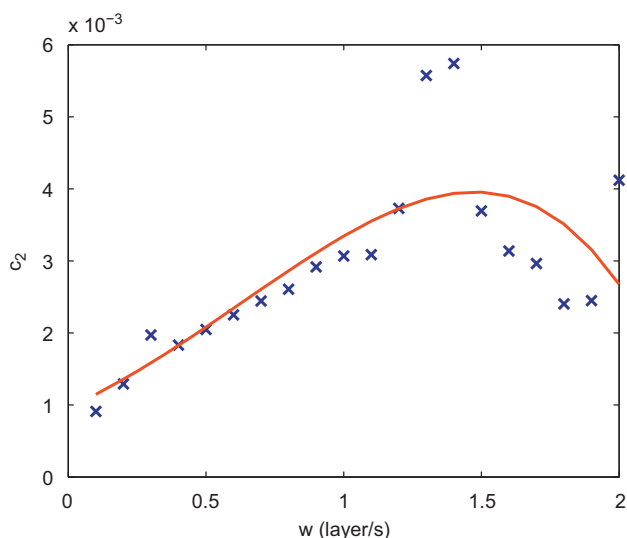


Fig. 11. c_2 values for different spatially uniform deposition rates w . The solid line is the result of a fourth-order polynomial fitting function and it is the c_2 versus w relationship used by the predictive controller.

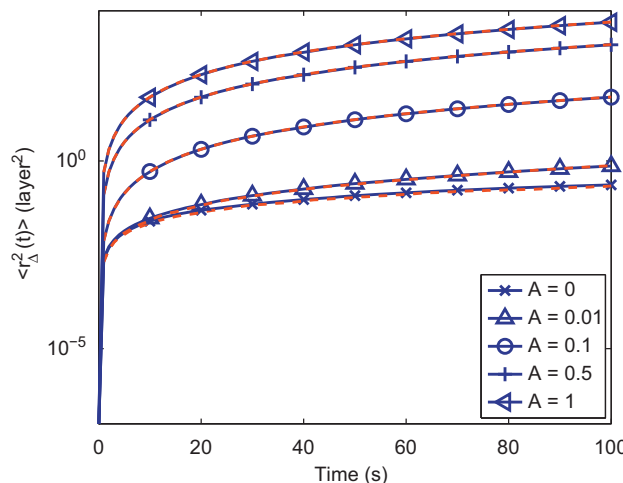


Fig. 13. Evolution of expected aggregate surface roughness for different patterned deposition magnitudes from the kMC model (solid lines with symbols) and expected aggregate roughness solutions from the corresponding EW equations (dashed lines). The c_2 and σ^2 values of the EW equations were estimated from open-loop aggregate surface roughness kMC model data with spatially uniform deposition rates.

σ^2 values obtained from these fitting results, polynomial functions are chosen to estimate c_2 and σ^2 values at different w_0 with the least-square method. Specifically, a fourth order polynomial function with respect to w_0 is chosen to estimate c_2 and a linear function is chosen to estimate σ^2 , and the expressions are given as follows:

$$c_2(w) = a_{c_2} w^4 + b_{c_2} w^3 + c_{c_2} w^2 + d_{c_2} w + e_{c_2},$$

$$\sigma^2 = a_{\sigma^2} w + b_{\sigma^2}, \quad (41)$$

where a_{c_2} , b_{c_2} , c_{c_2} , d_{c_2} , e_{c_2} , a_{σ^2} and b_{σ^2} are time-invariant fitting model parameters. The fitting results are shown in Figs. 11 and 12, where $a_{c_2} = -0.0003$, $b_{c_2} = -0.0002$, $c_{c_2} = 0.001$, $d_{c_2} = 0.0018$, $e_{c_2} = 0.001$, $a_{\sigma^2} = 0.8739$ and $b_{\sigma^2} = -0.0043$. These fitting results are based on kMC simulations with uniform deposition rate profiles ($A=0$). For simulations with patterned deposition rate profiles

($A \neq 0$), it is assumed that c_2 and σ^2 models obtained from uniform deposition rate simulations ($A=0$) can be used to estimate c_2 and σ^2 values. To verify this assumption, the solutions of EW equations for aggregate surface evolution with patterned deposition rate profile are obtained based on c_2 and σ^2 models from open-loop kMC data with uniform deposition rate, and these dynamic evolution profiles are compared with open-loop kMC dynamic evolution profiles with patterned deposition rate profiles. As shown in Figs. 13 and 14, c_2 and σ^2 models from open-loop kMC data with uniform deposition rate can be used in the EW equation to predict aggregate surface roughness and slope of the kMC model with patterned deposition rate. It is important to emphasize that the y-axes in Figs. 13 and 14 are logarithmic in order to make this comparison clear. We note that the approach presented for the computation of the parameters of the closed-form PDE model of Eq. (8) is not limited to the specific PDE system and can be used in the context of other dissipative PDE

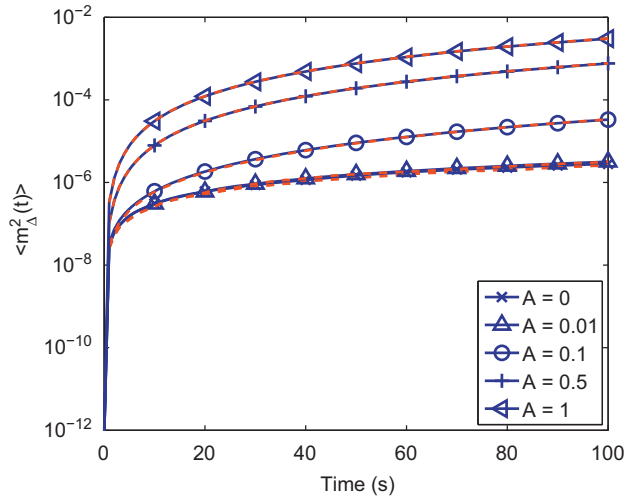


Fig. 14. Evolution of expected aggregate surface slope for different patterned deposition magnitudes from the kMC model (solid lines with symbols) and expected aggregate slope solutions from the corresponding EW equations (dashed lines). The c_2 and σ^2 values of the EW equations were estimated from open-loop aggregate surface roughness kMC model data with spatially uniform deposition rates.

systems that model the evolution of surface height of deposition processes. Finally, referring to the dependence of surface roughness and slope on lattice size, we note that both atomic and aggregate surface roughness and slope increase with increasing lattice size (this issue has been extensively studied in other works (Huang et al., 2010a, 2010b)); however, the proposed approach to closed-form modeling and MPC design is scalable and can be used in the context of different lattice size as long as the parameters of the stochastic PDE model of Eq. (8) and their dependence on deposition rate are computed on the basis of data obtained from the lattice size considered.

4. Model predictive control

In this section, we design a model predictive controller based on the dynamic models of aggregate surface roughness and slope to simultaneously control the expected values of aggregate surface roughness and slope square to desired levels. The dynamics of aggregate surface roughness and slope of the thin film are described by the EW equation of aggregate surface height of Eq. (8) with the computed parameters of Subsection 3.4. State feedback control is considered in this work, i.e., $h_A(x,t)$ is assumed to be available for feedback. In practice, real-time surface height measurements can be obtained via atomic force microscopy (AFM) systems.

4.1. MPC formulation for regulation of aggregate roughness and slope

We consider the problem of regulation of aggregate surface roughness and slope to desired levels within a model predictive control framework. Due to the stochastic nature of the variables, the expected values of aggregate surface roughness and slope, $\langle r_A^2(t) \rangle$ and $\langle m_A^2(t) \rangle$, are chosen as the control objectives. The mean deposition rate, w_0 , and magnitude of patterned deposition rate, A , are chosen as the manipulated inputs; the substrate temperature is fixed at $T=480$ K during all closed-loop simulations. To account for a number of practical considerations, several constraints are added to the control problem. In particular, since

$w(x) \geq 0$, the constraint $0 \leq A \leq w_0$ is imposed to ensure $w(x,t) > 0$, $\forall(x,t)$. To ensure the validity of the closed-form process model, there is a constraint on the range of variation of the mean deposition rate. Another constraint is imposed on the rate of change of the mean deposition rate to account for actuator limitations. The control action at time t is obtained by solving a finite-horizon optimal control problem. The cost function in the optimal control problem includes penalty on the deviation of $\langle r_A^2 \rangle$ and $\langle m_A^2 \rangle$ from their respective set-point values. Different weighting factors are assigned to the aggregate surface roughness and slope. Aggregate surface roughness and slope have very different magnitudes, ($\langle r_A^2 \rangle$ ranges from 10^2 to 10^4 and $\langle m_A^2 \rangle$ ranges from 10^{-5} to 10^{-2}). Therefore, relative deviations are used in the formulation of the cost function to make the magnitude of the two terms comparable in the cost function. The optimization problem is subject to the dynamics of the aggregate surface height of Eq. (8). The optimal w_0 and A values are calculated at each sampling time by solving a finite-dimensional optimization problem in a receding horizon fashion. Specifically, the MPC problem at time t is formulated as follows:

$$\min_{w_0, A} f(w_0, A) = q_{r^2} \left[\frac{r_{set}^2 - \langle r_A^2(t_f) \rangle}{r_{set}^2} \right]^2 + q_{m^2} \left[\frac{m_{set}^2 - \langle m_A^2(t_f) \rangle}{m_{set}^2} \right]^2, \quad (42)$$

where

$$\langle r_A^2(t_f) \rangle = \frac{1}{L} \sum_{n=1}^{L/(2A)} \sum_{p=1}^2 \langle z_{p,n}^2(t_f) \rangle, \quad (43)$$

$$\langle m_A^2(t_f) \rangle = \sum_{n=1}^{L/(2A)} \sum_{p=1}^2 (K_{p,n} \langle z_{p,n}^2(t_f) \rangle), \quad (43)$$

$$\langle z_{p,n}^2(t_f) \rangle = \text{var}(z_{p,n}(t_f)) + \langle z_{p,n}(t_f) \rangle^2, \quad (44)$$

$$\langle z_{p,n}(t_f) \rangle = e^{\lambda_n(t_f-t)} \langle z_{p,n}(t) \rangle + \frac{W_p}{\lambda_n} (e^{\lambda_n(t_f-t)} - 1), \quad (45)$$

$$\text{var}(z_{p,n}(t_f)) = e^{2\lambda_n(t_f-t)} \text{var}(z_{p,n}(t)) + \sigma^2(w) \frac{e^{2\lambda_n(t_f-t)} - 1}{2\lambda_n}, \quad (46)$$

$$\lambda_n = -\frac{4c_2(w)\pi^2}{L^2} n^2 \quad (47)$$

and

$$c_2(w) = a_{c_2} w^4 + b_{c_2} w^3 + c_{c_2} w^2 + d_{c_2} w + e_{c_2}, \quad (48)$$

$$\sigma^2(w) = a_{\sigma^2} w + b_{\sigma^2} \quad (49)$$

subject to:

$$w_{min} \leq w_0 \leq w_{max}, \quad |w_0(t) - w_0(t-dt)| \leq \delta w_{max}, \quad (50)$$

$$w = w_0 + A \sin\left(\frac{k\pi x}{L}\right), \quad 0 \leq A \leq w_0, \quad (51)$$

where t is the current time, dt is the sampling time, q_{r^2} and q_{m^2} are the weighting penalty factors for the deviations of $\langle r_A^2 \rangle$ and $\langle m_A^2 \rangle$ from their respective set-points at the i th prediction step, w_{min} and w_{max} are the lower and upper bounds on the mean deposition rate, respectively, and δw_{max} is the limit on the rate of change of the mean deposition rate. Given the batch nature of the deposition process, the MPC of Eq. (42) includes penalty on the discrepancy of the expected surface roughness and slope at the end of the deposition from the set-points values of surface roughness and slope that lead to desired film reflectance levels.

The optimal control actions are obtained from the solution of the multivariable optimization problem of Eq. (42), and are applied to the deposition process model over dt (i.e., either the EW equation model or the kMC model) during the time interval $(t, t+dt)$. At time $t+dt$,

a new measurement of aggregate surface roughness and slope is received by the controller and the MPC problem of Eq. (42) is solved for the next set of control actions. An interior point method optimizer, IPOPT (Wächter and Biegler, 2006), is used to solve the optimization problem in the MPC formulation. With respect to the stability of the closed-loop system, we note the following: the deposition process considered including atom adsorption and atom migration is an inherently stable process; this is evident by the negative values of all the eigenvalues of the spatial differential operator of the Edwards–Wilkinson-type equation (Eq. (8)) used to model the evolution of surface height for all values of the deposition rate. Given this stability property of the open-loop process and the specific MPC design, the stability of the closed-loop system is ensured.

5. Simulation results

In this section, the model predictive controller of Eq. (42) is applied to both the one-dimensional EW equation-type model of Eq. (8) and the one-dimensional kMC model of the thin film growth process. The mean deposition rate ranges from 0.1 to 2 layer/s, the substrate temperature is fixed at 480 K, the lattice size of the kMC model is fixed at 40,000 sites, the aggregation size is fixed at 400 to make the results relevant to thin film solar cell applications and five sine waves are used in the patterned deposition rate profile. The sampling time is 5 s; this sampling time is enough for the MPC to carry out the calculations needed to compute the control action. In addition to the deposition rate, the temperature may be used as a manipulated input but it should vary in space to induce substantial aggregate surface roughness and slope values at spatial scales corresponding to the visible light wavelength. Each closed-loop simulation lasts for 100 s. Expected values are calculated from 100 independent closed-loop system simulation runs. In all the simulations, the aggregate surface roughness and slope set-points remain the same, specifically, $r_{set}^2 = 10,000$ and $m_{set}^2 = 0.002$.

5.1. MPC application to EW equation model

In this subsection, the EW equation model is utilized in the closed-loop control problem as the plant model. First, the problem of regulating aggregate surface roughness is considered. In this problem, the cost function has only penalty on the deviation of the expected aggregate surface roughness square from its set-point, i.e., $q_{r^2} = 1$ and $q_{m^2} = 0$. Fig. 15 shows the evolution profile of $\langle r_A^2(t) \rangle$

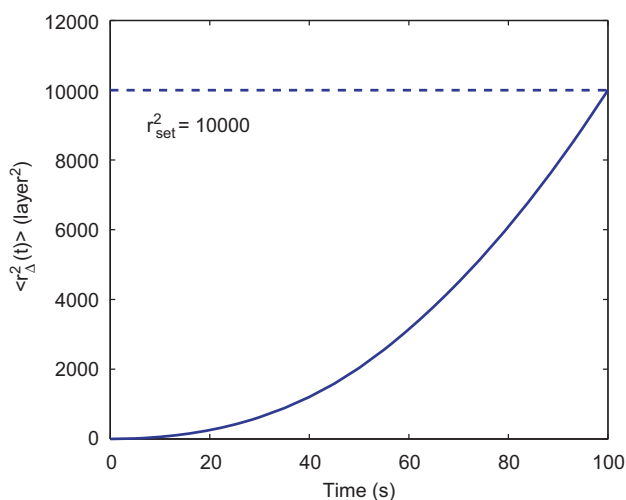


Fig. 15. Profile of expected aggregate surface roughness square with EW equation as the plant model. $q_{r^2} = 1$, $q_{m^2} = 0$ and $r_{set}^2 = 10,000$.

under the model predictive controller of Eq. (42). It is clear that the controller drives the expected aggregate surface roughness to its set-point at the end of the simulation. Fig. 16 shows the input profiles of w_0 and A for these simulations. It is necessary to point out that during the first half of the simulation time, the optimal solutions of w_0 are constrained by the rate of change constraint and the optimal solutions of A are bounded by the values of w_0 .

Next, the aggregate surface slope is regulated. The cost function includes only penalty on the deviation of the expected value of aggregate surface slope square from its set-point ($q_{m^2} = 1$, $q_{r^2} = 0$). Fig. 17 shows the evolution profile of the expected aggregate slope square. The aggregate slope reaches its set-point at $t=100$ s. Fig. 18 displays the input profile in this scenario. Compared with Fig. 16, the controller requires less time to find the input values needed to reach the desired slope value.

The next step is the simultaneous regulation of aggregate surface roughness and slope. The weighting factor of aggregate slope square, q_{m^2} , is kept at 1, while the weighting factor of aggregate roughness square, q_{r^2} , increases from 10^{-2} to 10^3 . Fig. 19 shows the values of expected aggregate surface roughness and slope at the end of

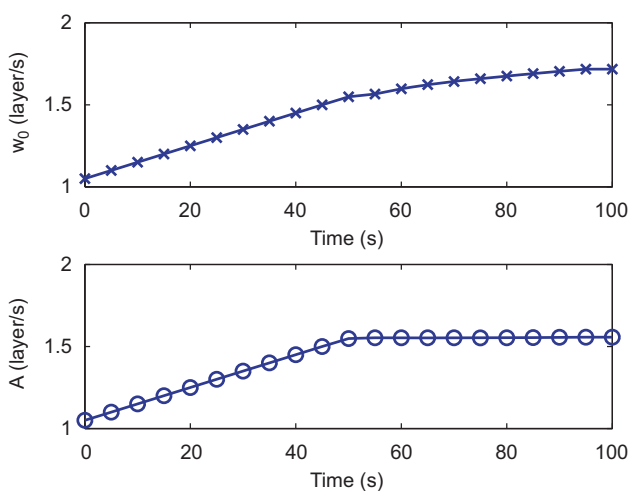


Fig. 16. Input profiles for aggregate roughness-only control problem with EW equation as the plant model. $q_{r^2} = 1$, $q_{m^2} = 0$ and $r_{set}^2 = 10,000$.

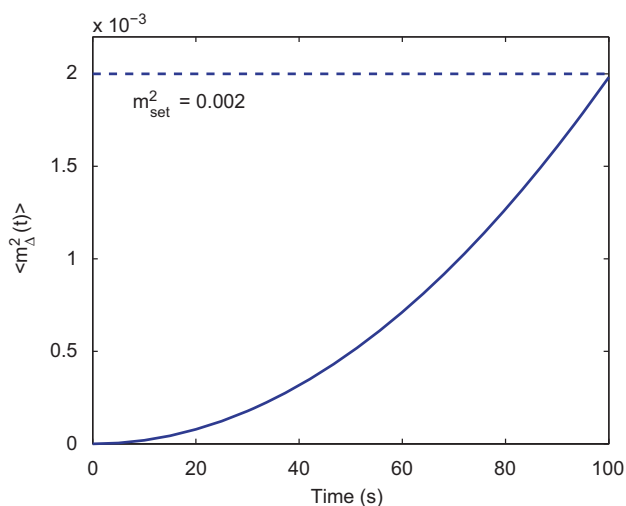


Fig. 17. Profile of expected aggregate surface slope square with EW equation as the plant model. $q_{r^2} = 0$, $q_{m^2} = 1$ and $m_{set}^2 = 0.002$.

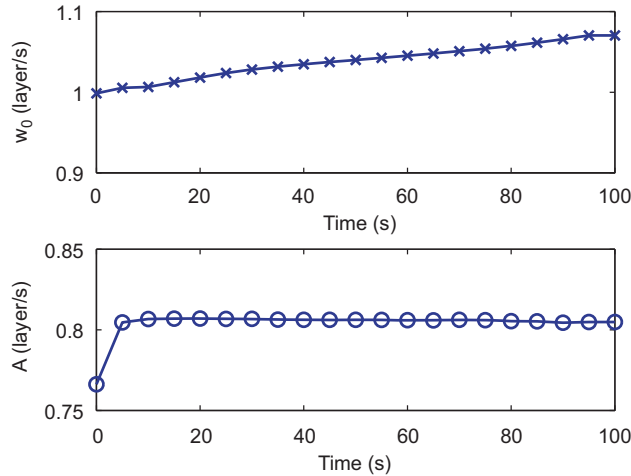


Fig. 18. Input profiles for aggregate slope-only control problem with EW equation as the plant model. $q_{r^2} = 0$, $q_{m^2} = 1$ and $m_{set}^2 = 0.002$.

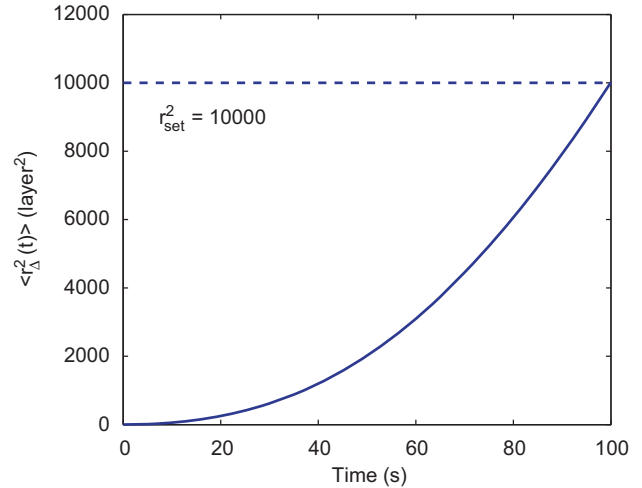


Fig. 20. Profile of expected aggregate surface roughness square with kMC model as the plant model. $q_{r^2} = 1$, $q_{m^2} = 0$ and $r_{set}^2 = 10,000$.

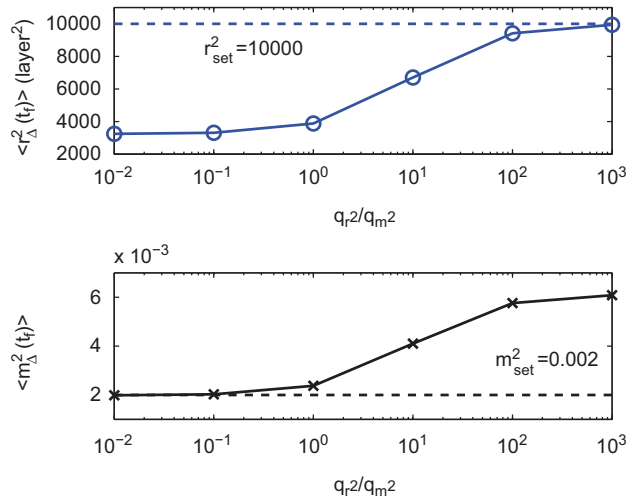


Fig. 19. $\langle r_{\Delta}^2(t_f) \rangle$ and $\langle m_{\Delta}^2(t_f) \rangle$ at the end of closed-loop simulations ($t = 100$ s) for different penalty weighting factors in the predictive controller with EW equation as the plant model. $10^{-2} \leq q_{r^2} \leq 10^3$, $q_{m^2} = 1$, $r_{set}^2 = 10,000$ and $m_{set}^2 = 0.002$.

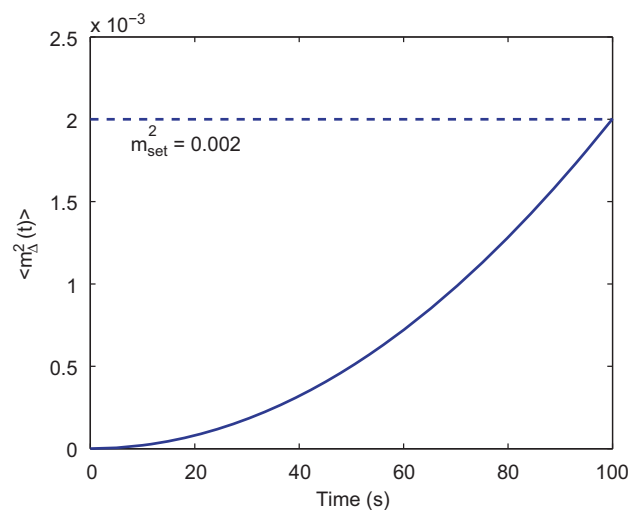


Fig. 21. Profile of expected aggregate surface slope square with kMC model as the plant model. $q_{r^2} = 0$, $q_{m^2} = 1$ and $m_{set}^2 = 0.002$.

closed-loop simulations ($t_f = 100$ s) as a function of q_{r^2}/q_{m^2} . It can be seen that as the weighting on aggregate roughness increases, the expected value of aggregate roughness approaches its set-point at the cost of larger deviation of the aggregate slope from its set-point.

5.2. MPC application to kMC model

In this subsection, the kMC model is used in the closed-loop control problem as the plant model, while all the other settings remain the same. Fig. 20 shows the aggregate surface roughness in the case of roughness-only control while Fig. 21 shows the aggregate surface slope in the case of slope-only control. From both plots, we see that both aggregate roughness and slope successfully reach their set-points at the end of the simulations. Furthermore, the closed-loop evolution profiles with kMC as the plant model are very similar to the closed-loop profiles that use the EW equation as the plant model, which implies that the EW equation model used in this work can accurately predict the kMC simulation results.

Simultaneous regulation of aggregate surface roughness and slope has also been investigated. Similar to the case where the EW equation is used as the plant model, the weighting factor of aggregate slope square, q_{m^2} , is kept at 1, and the weighting factor of aggregate roughness square, q_{r^2} , ranges from 10^{-2} to 10^3 . Fig. 22 shows the values of expected aggregate roughness and slope at the end of simulations as a function of q_{r^2}/q_{m^2} . It can be seen that the expected value of aggregate roughness approaches its set-point as q_{r^2} increases at the cost of larger deviation of the aggregate slope from its set-point.

5.3. Application to light trapping efficiency

In this subsection, we demonstrate an application of the proposed modeling and control framework to improve thin film solar cell performance. When the incident light goes through a rough interface, the light is divided into four components: specular reflection, specular transmission, diffused reflection, and diffused transmission (Tao and Zeman, 1994; Leblanc and Perrin, 1994). The total reflectance of a beam of monochromatic light at normal

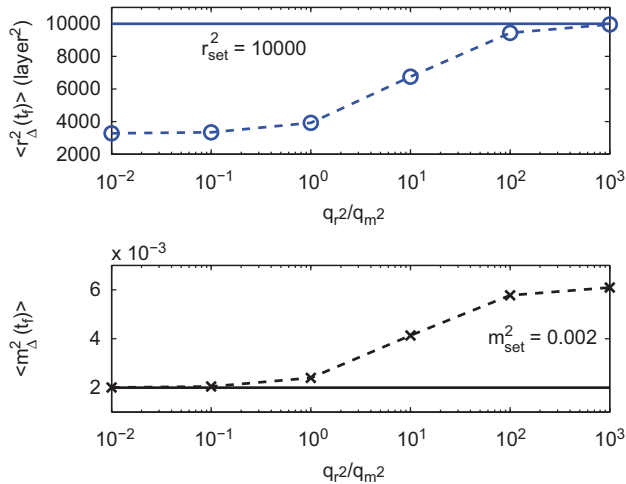


Fig. 22. $\langle r_{\Delta}^2(t_f) \rangle$ and $\langle m_{\Delta}^2(t_f) \rangle$ at the end of closed-loop simulations ($t=100$ s) for different penalty weighting factors in the predictive controller with kMC model as the plant model. $10^{-2} \leq q_{r^2} \leq 10^3$, $q_{m^2} = 1$, $r_{set}^2 = 10,000$ and $m_{set}^2 = 0.002$.

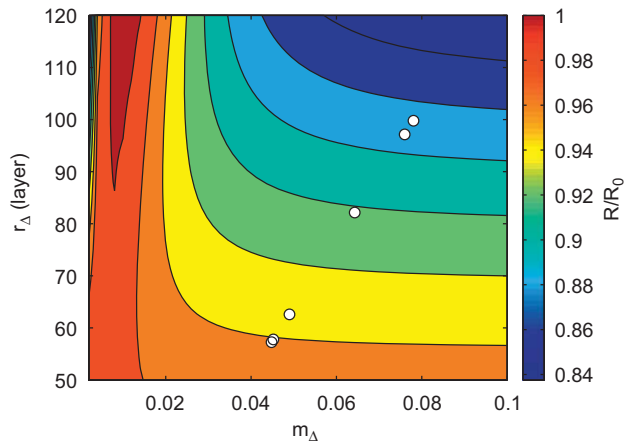


Fig. 23. Light reflectance of thin films deposited under closed-loop operations with different weighting factor ratios. $q_{r^2} = 10^{-2}, 10^{-1}, 10^0, 10^1, 10^2$ and 10^3 (corresponding to small circles inside the figure from left to right), $q_{m^2} = 1$, $r_{set}^2 = 10,000$ and $m_{set}^2 = 0.002$.

incidence to a rough surface, which is denoted by R , can be approximately calculated as follows (Davies, 1954):

$$R = R_0 \exp\left(-\frac{4\pi r_{\Delta}^2}{\lambda^2}\right) + R_0 \int_0^{\pi/20} 2\pi^4 \left(\frac{a_{\Delta}}{\lambda}\right)^2 \left(\frac{r_{\Delta}}{\lambda}\right)^2 (\cos \theta + 1)^4 \sin \theta \exp\left[-\frac{(\pi a \sin \theta)^2}{\lambda^2}\right] d\theta, \quad (52)$$

where R_0 is the reflectance of a perfectly smooth surface of the same material, λ is the light wavelength, a_{Δ} is the auto-covariance length of the interface, which can be rewritten as a ratio between the aggregate roughness and aggregate slope as $a_{\Delta} = \sqrt{2}r_{\Delta}/m_{\Delta}$ (Bennett and Porteus, 1961), and θ is the incident angle. Eq. (52) is only valid when θ is small (Davies, 1954), so the integration upper limit of θ is assumed to be $\pi/20$. Furthermore, aggregate roughness and slope at aggregation length $\Delta = 400$ are used in Eq. (52).

Fig. 23 shows how films with different reflectance values can be produced by simultaneous regulation of film surface aggregate roughness and aggregate slope. Specifically, the weighting factor

of aggregate slope square, q_{m^2} , is kept at 1, and the weighting factor of aggregate roughness square, q_{r^2} , ranges from 10^{-2} to 10^3 , and the resulting aggregate roughness and slope are used to compute the light reflectance of the thin film according to Eq. (52). It is clear that films with different reflectance values can be generated by regulating aggregate surface roughness and slope; please see the small circles in Fig. 23.

Remark 1. Referring to the model predictive controller of Eq. (42), we note that in the absence of measurement feedback it can still be used to compute in an open-loop fashion an input trajectory for manipulating the deposition rate profile to drive the surface roughness and slope to desired levels at the end of the deposition; however, such an approach is inherently non-robust to process disturbances and model uncertainty owing to the lack of feedback. Furthermore, when measurements of the film surface height are available at specific locations across the film surface, a state estimator based on the stochastic PDE model can be used to provide estimates of the entire film thickness; these estimates can be subsequently used in the model predictive controller of Eq. (42). Finally, we note that even though the controller of Eq. (42) focuses on the regulation of surface roughness and slope at desired levels, it is possible to incorporate in the controller additional objectives like, for example, achieving a desired film thickness; this can be done by the incorporation of additional thickness requirement constraints in the controller to ensure that the deposition rate is above a certain value that ensures that final film thickness is achieved at the end of the deposition that meets the specifications.

6. Conclusions

In this work, a thin film deposition process is simulated via a kinetic Monte Carlo method in a large lattice ($L=40,000$) and a patterned deposition rate profile is introduced to generate significant aggregate surface roughness and slope at a length scale comparable to the wavelength of visible light. An Edwards–Wilkinson-type equation for the aggregate surface profile is used to predict the surface temporal evolution of aggregate surface roughness and slope. A model predictive controller is designed to regulate aggregate surface roughness and slope to desired levels, and the controller is applied to the EW equation and the kMC model of the deposition process with $L=40,000$. Simulation results demonstrate the applicability and effectiveness of the controller and of the spatially-patterned deposition rate profile by demonstrating that different thin film reflectance values can be generated by successfully controlling aggregate roughness and slope to desired values.

Acknowledgments

Financial support from the National Science Foundation, CBET-0652131, and UCLA Doctoral Dissertation Year Fellowships for Xinyu Zhang and Jianqiao Huang are gratefully acknowledged.

References

Bennett, H.E., Porteus, J.O., 1961. Relation between surface roughness and specular reflectance at normal incidence. *Journal of the Optical Society of America* 51, 123–129.
 Buzea, C., Robbie, K., 2005. State of the art in thin film thickness and deposition rate monitoring sensors. *Reports on Progress in Physics* 68, 385–409.
 Christofides, P.D., 2001. *Nonlinear and Robust Control of PDE Systems: Methods and Applications to Transport-Reaction Processes*. Birkhäuser, Boston.
 Christofides, P.D., Armaou, A., Lou, Y., Varshney, A., 2008. *Control and Optimization of Multiscale Process Systems*. Birkhäuser, Boston.

- Davies, H., 1954. The reflection of electromagnetic waves from a rough surface. *Proceedings of the IEE—Part IV: Institution Monographs* 101, 209–214.
- Edwards, S.F., Wilkinson, D.R., 1982. The surface statistics of a granular aggregate. *Proceedings of the Royal Society of London Series A—Mathematical Physical and Engineering Sciences* 381, 17–31.
- Gillespie, D.T., 1976. A general method for numerically simulating the stochastic time evolution of coupled chemical reactions. *Journal of Computational Physics* 22, 403–434.
- Green, M.A., 2007. Thin-film solar cells: review of materials, technologies and commercial status. *Journal of Materials Science: Materials in Electronics* 18, 15–19.
- Hu, G., Huang, J., Orkoulas, G., Christofides, P.D., 2009a. Investigation of film surface roughness and porosity dependence on lattice size in a porous thin film deposition process. *Physical Review E* 80, 041122.
- Hu, G., Orkoulas, G., Christofides, P.D., 2009b. Modeling and control of film porosity in thin film deposition. *Chemical Engineering Science* 64, 3668–3682.
- Hu, G., Orkoulas, G., Christofides, P.D., 2009c. Regulation of film thickness, surface roughness and porosity in thin film growth using deposition rate. *Chemical Engineering Science* 64, 3903–3913.
- Huang, J., Hu, G., Orkoulas, G., Christofides, P.D., 2010a. Dependence of film surface roughness and slope on surface migration and lattice size in thin film deposition processes. *Chemical Engineering Science* 65, 6101–6111.
- Huang, J., Hu, G., Orkoulas, G., Christofides, P.D., 2010b. Dynamics and lattice-size dependence of surface mean slope in thin-film deposition. *Industrial & Engineering Chemistry Research* 50, 1219–1230.
- Isabella, O., Krč, J., Zeman, M., 2010. Modulated surface textures for enhanced light trapping in thin-film silicon solar cells. *Applied Physics Letters* 97, 101106.
- Krč, J., Zeman, M., 2002. Experimental investigation and modelling of light scattering in a-si:h solar cells deposited on glass/zno:al substrates. *Material Research Society Proceedings* 715.
- Lauritsen, K.B., Cuerno, R., Makse, H.A., 1996. Noisy Kuramoto–Sivashinsky equation for an erosion model. *Physical Review E* 54, 3577–3580.
- Leblanc, F., Perrin, J., 1994. Numerical modeling of the optical properties of hydrogenated amorphous-silicon-based p-i-n solar cells deposited on rough transparent conducting oxide substrates. *Journal of Applied Physics* 75, 1074–1086.
- Levine, S.W., Clancy, P., 2000. A simple model for the growth of polycrystalline Si using the kinetic Monte Carlo simulation. *Modelling and Simulation in Materials Science and Engineering* 8, 751–762.
- Levine, S.W., Engstrom, J.R., Clancy, P., 1998. A kinetic Monte Carlo study of the growth of Si on Si(100) at varying angles of incident deposition. *Surface Science* 401, 112–123.
- Muller, J., Rech, B., 2004. TCO and light trapping in silicon thin film solar cells. *Solar Energy* 77, 917–930.
- Ni, D., Christofides, P.D., 2005. Multivariable predictive control of thin film deposition using a stochastic PDE model. *Industrial & Engineering Chemistry Research* 44, 2416–2427.
- Poruba, A., Fejfar, A., Remeš, Z., Špringer, J., Vaněček, M., Kočka, J., 2000. Optical absorption and light scattering in microcrystalline silicon thin films and solar cells. *Journal of Applied Physics* 88, 148–160.
- Reese, J.S., Raimondeau, S., Vlachos, D.G., 2001. Monte Carlo algorithms for complex surface reaction mechanisms: efficiency and accuracy. *Journal of Computational Physics* 173, 302–321.
- Rowlands, S.F., Livingstone, J., Lund, C.P., 2004. Optical modelling of thin film solar cells with textured interface using the effective medium approximation. *Solar Energy* 76, 301–307.
- Springer, J., Poruba, A., 2001. Improved optical model for thin film silicon solar cells. In: *Seventeenth European Photovoltaic Solar Energy Conference*, vol. 0, pp. 11.
- Tao, G., Zeman, M., 1994. Optical modeling of a-si:h based solar cells on textured substrates. In: *1994 IEEE First World Conference on Photovoltaic Energy Conversion. Conference Record of the Twenty Fourth IEEE Photovoltaic Specialists Conference-1994 (Cat.No.94CH3365-4)*, vol. 1, pp. 666.
- van Sark, W., Brandsen, G.W., Fleuster, M., Hekkert, M.P., 2007. Analysis of the silicon market: will thin films profit? *Energy Policy* 35, 3125–3221.
- Varshney, A., Armaou, A., 2005. Multiscale optimization using hybrid PDE/kMC process systems with application to thin film growth. *Chemical Engineering Science* 60, 6780–6794.
- Varshney, A., Armaou, A., 2006. Optimal operation of GaN thin-film epitaxy employing control vector parametrization. *AIChE Journal* 52, 1378–1391.
- Vorburger, T.V., Marx, E., Lettieri, T.R., 1993. Regimes of surface-roughness measurable with light-scattering. *Applied Optics* 32, 3401–3408.
- Vvedensky, D.D., Zangwill, A., Luse, C.N., Wilby, M.R., 1993. Stochastic equations of motion for epitaxial growth. *Physical Review E* 48, 852–862.
- Wächter, A., Biegler, L.T., 2006. On the implementation of an interior-point filter line-search algorithm for large-scale nonlinear programming. *Mathematical Programming* 106 (1), 25–57.
- Wang, L., Clancy, P., 2001. Kinetic Monte Carlo simulation of the growth of polycrystalline Cu films. *Surface Science* 473, 25–38.
- Yang, Y.G., Johnson, R.A., Wadley, H.N., 1997. A Monte Carlo simulation of the physical vapor deposition of nickel. *Acta Materialia* 45, 1455–1468.
- Zeman, M., Vanswaaij, R., 2000. Optical modeling of a-Si: H solar cells with rough interfaces: effect of back contact and interface roughness. *Journal of Applied Physics* 88, 6436–6443.
- Zhang, X., Hu, G., Orkoulas, G., Christofides, P.D., 2010a. Multivariable model predictive control of thin film surface roughness and slope for light trapping optimization. *Ind. & Eng. Chem. Res* 49, 10510–10516.
- Zhang, X., Hu, G., Orkoulas, G., Christofides, P.D., 2010b. Predictive control of surface mean slope and roughness in a thin film deposition process. *Chemical Engineering Science* 65, 4720–4731.
- Zhang, X., Huang, J., Hu, G., Orkoulas, G., Christofides, P.D. Controlling aggregate thin film surface morphology for improved light trapping using a patterned deposition rate profile. *Chemical Engineering Science*, in press. doi: 10.1016/j.ces.2011.03.047.